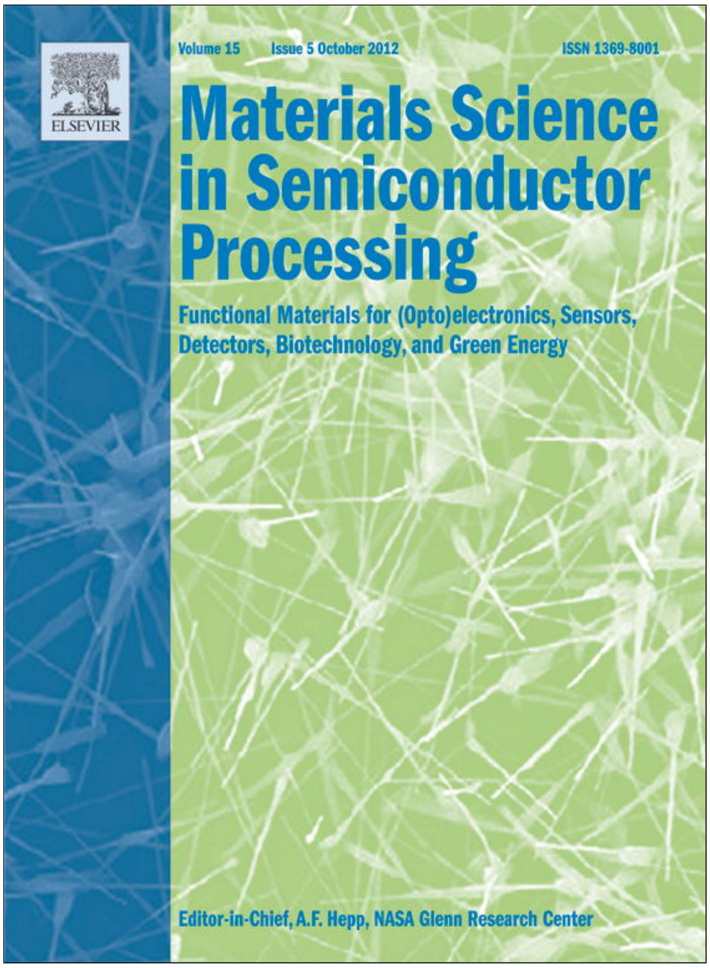
Volume 15
Issue 5 October 2012
ISSN 1369-8001
ELSEVIER
Materials Science in Semiconductor Processing
Functional Materials for (Opto)electronics, Sensors, Detectors, Biotechnology, and Green Energy
Editor-in-Chief, A.F. Hepp, NASA Glenn Research Center

Materials Science in Semiconductor Processing 15 (2012) 549–554

Contents lists available at SciVerse ScienceDirect

Materials Science in Semiconductor Processing

journal homepage: www.elsevier.com/locate/mssp

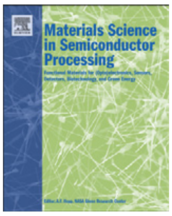

# Characterizations of solid-state microwave-synthesized $Sb_2Te_3$-based alloys with various compositions of bismuth in $Bi_{2x}Sb_{2(1-x)}Te_3$

A. Kadhim*, A. Hmood, H. Abu Hassan

*Nano-Optoelectronic Research and Technology Laboratory (N.O.R.), School of Physics, Universiti Sains Malaysia, 11800 Pulau Penang, Malaysia*

ARTICLE INFO

Available online 30 April 2012

*Keywords:*
Microwave irradiation
Chalcogenides
Electrical properties
Crystal structure

ABSTRACT

In this article, thermoelectric (TE) materials based on p-type $Sb_2Te_3$ samples and dispersed with $x$ amounts of Bi ($x=0.0$, 0.2, 0.4, 0.6, 0.8, and 1.0) in the form $Bi_{2x}Sb_{2(1-x)}Te_3$ were synthesized via a standard solid-state microwave route. The microstructure of the ingots was characterized by field emission scanning electron microscopy. As-synthesized ingots were formed by the assembly of micro-sheet grains. The phase composition of the powders was characterized by X-ray diffraction, revealing a rhombohedral structure. The influence of variations in Bi content ($x$) on the TE properties of the resulting alloy was studied in the temperature range of 303 K to 523 K. Increases in $x$ caused a decrease in hole concentration and electrical conductivity and an increase in Seebeck coefficient. A maximum power factor of 4.96 mW/mK$^2$ was obtained at about 373 K for a $Bi_{2x}Sb_{2(1-x)}Te_3$ sample with $x=0.2$.

## 1. Introduction

The performance of thermoelectric (TE) materials is determined by a dimensionless figure of merit ($ZT$), which is a function involving electrical conductivity ($\sigma$), the Seebeck coefficient ($S$), and thermal conductivity ($k$) in the relationship $ZT=S^2\sigma T/k$. Electrical properties are determined by the power factor, given by $\sigma S^2$. The total $k$ is contributed to by two values: one from the electrical carrier $k_e$ and another from the lattice thermal vibration $k_{ph}$.

TE materials must feature a high power factor and low $k$ to exhibit high performance. This power factor can be optimized as a function of the carrier concentration. Therefore, $k$ must be reduced to maximize $ZT$ [1,2].

The complex crystal structures and disordered atomic distributions of $Sb_2Te_3$ and $Bi_2Te_3$ bring about exceptionally low lattice $k$, significantly contributing to their excellent TE properties [3]. These materials show TE anisotropy originating from their structural anisotropy, as having a layered hexagonal structure comprised of five atomic stacks in the $Te_1$–Bi–$Te_2$–Bi–$Te_1$ form. Te1–Te1 layers are bonded by weak Van der Waals forces [4]. Over the last few years, many TE devices have been built using bismuth telluride and its alloys. In the application of Bi–Te– or Bi–Sb-based alloys, preparation of effective materials with well-defined physical parameters (e.g., $S$, $\sigma$, $k$, and mobility of free carriers) [5] is crucial. Several interdependent parameters must be considered when adjusting the properties of TE materials. Simply put, $\sigma$ and the electronic contribution of a material to $k$ depend on its electronic structure [6]. A number of techniques have been developed for the fabrication of Bi–Te alloys, including the Bridgman technique [7] and powder metallurgy technologies [8–11], such as sintering of pulverized and intermixed elements, mechanical alloying and hot pressing, vapor–liquid–solid growth [12], and rapid solid-state microwave synthesis [13,14]. Solid-state microwave synthesis is a rapid, simple, and economically feasible method of preparing binary group chalcogenides, such as $Sb_2Te_3$ and $Bi_2Te_3$. The advantage of synthesizing inorganic compounds via solid-state microwaves over more traditional methods is that the materials obtained from

---

* Corresponding author. Tel.: +60174519357; fax: +6046579150.
*E-mail address:* areejkadhim@yahoo.com (A. Kadhim).

1369-8001/$ - see front matter © 2012 Elsevier Ltd. All rights reserved.
http://dx.doi.org/10.1016/j.mssp.2012.04.006

the former can exhibit different morphologies and microstructures compared with those obtained from the latter [15]. Samples prepared using microwaves have been shown to possess enhanced physical properties compared with materials synthesized using other techniques [16], have dramatically reduced reaction times, and feature no solvent waste. Thus, solid-state microwave synthesis is an easy, energy-efficient, and relatively green method of preparing technologically useful solid-state inorganic materials [17]. To the best of our knowledge, studies measuring the TE properties of a mixture with $Sb_2Te_3$ and $Bi_2Te_3$, such as $Bi_{2x}Sb_{2(1-x)}Te_3$ prepared via solid-state microwave synthesis, have yet to be reported. In the current study, $Sb_2Te_3$ and $Bi_2Te_3$, both of which are identified as excellent inorganic microwave absorbers, were used to synthesize polycrystalline ternary compounds of $Bi_{2x}Sb_{2(1-x)}Te_3$ within 10 min at 2.45 GHz and 800 W. The structural and TE properties of $Bi_{2x}Sb_{2(1-x)}Te_3$ ($x$=0.0, 0.2, 0.4, 0.6, 0.8, and 1.0) were then studied.

## 2. Experimental

### 2.1. Sample preparation

The Bi, Sb, and Te samples used in this research were of high purity (99.999%). $Sb_2Te_3$ (2 g) was prepared by mixing Sb (0.7776 g) with Te (1.2224 g). $Bi_2Te_3$ (2 g) was obtained by mixing Bi (1.04391 g) with Te (0.95609 g) at a molar ratio of 2:3. All elements were weighed based on the formula $Bi_{2x}Sb_{2(1-x)}Te_3$ ($x$=0.0, 0.2, 0.4, 0.6, 0.8, and 1.0). Fig. 1 shows the preparation of $Sb_2Te_3$ ingots via solid-state microwave synthesis. All elements were mixed, ground for 20 min using a mortar and a pestle, and then placed inside a 12 mm (O.D) × 10 mm (I.D) quartz ampule under a $10^{-5}$ mbar vacuum. The ampule was inserted into a holder, which kept the sample in a vertical orientation inside the microwave oven. The sample was irradiated in an 800 W MS2147C microwave oven (LG) at 2.45 GHz for 10 min, with shaking every minute to ensure that the composition was homogeneous. The sample was subjected to irradiation intervals at 100% power. After microwave irradiation, the reaction ampules were opened, and the products were removed and examined.

### 2.2. Physical measurements

Selected portions of the ingots were imaged by field emission scanning electron microscopy (FESEM)(LEO SUPRA 50VP, Carl Zeiss, Germany). X-ray diffraction (XRD) patterns of the resultant powders were recorded using an X-ray diffractometer system (PANalytical X'Pert PRO MRD PW3040, Almelo, The Netherlands) operated at 40 kV, 30 mA, and Cu$K_\alpha$ radiation. $Bi_{2x}Sb_{2(1-x)}Te_3$ powders were then pressed into disk shapes (diameter, 13 mm; thickness, 0.58 mm) by cold pressing at 10 t. Density was measured using Archimedes' method. $S$ and $k$ were measured via the standard four-probe DC method under a vacuum of $10^{-3}$ mbar from room temperature to about 523 K. The Hall coefficient ($R_H$) was determined at room temperature with an applied magnetic field of

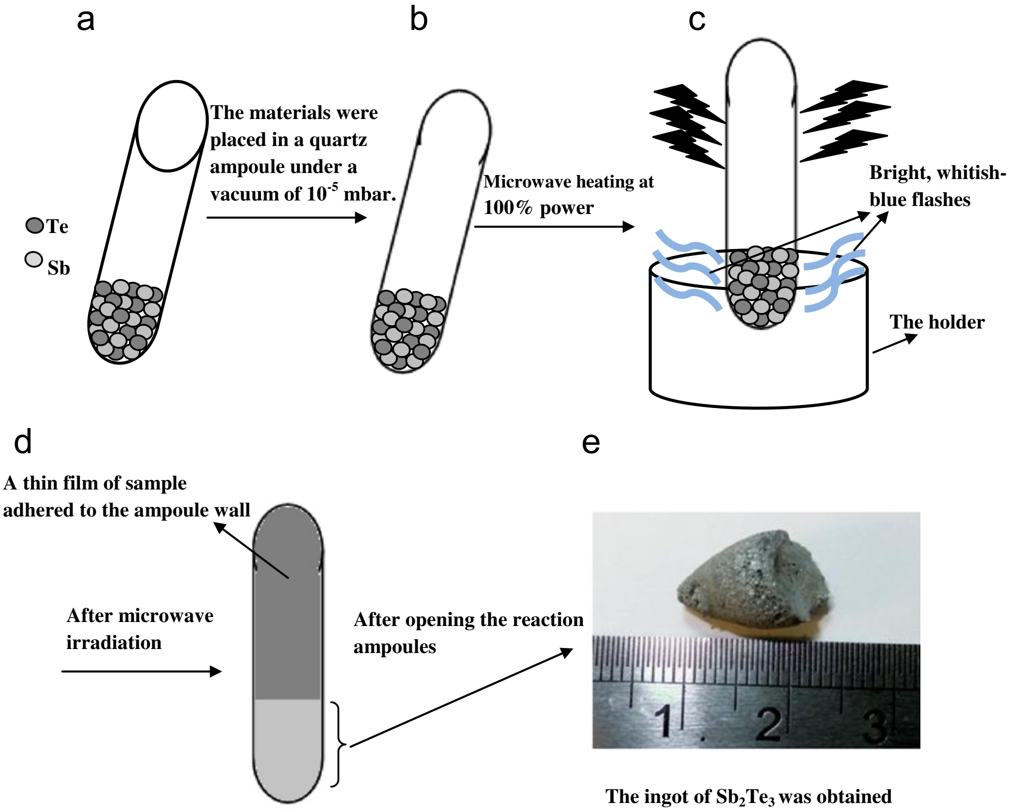

**Fig. 1.** Schematic of microwave synthesis of $Sb_2Te_3$.

1 T using a Model 637 electromagnetic power supply (Lake Shore Cryotronics, Inc. USA).

## 3. Results and discussion

### 3.1. Microwave synthesis mechanism

Bright, whitish-blue plasma was observed emerging from all of the ampules from the first minute of microwave exposure. During microwave irradiation, a thin film of the sample adhered to the walls of the ampules. The amount and thickness of the film depended on the reaction. Silvery-gray products typically took on the shape of their quartz reaction ampules, as shown in Fig. 1. The final synthesized materials showed a complete reaction process (Fig. 1(e)). This finding is in accordance with a small quantity of the sample used, and this quantity is important for solid-state microwave reactions especially for microwave penetration depth. During exposure to microwaves, the incident microwave power is reduced from its original value to about half as the depth of penetration of a material increases. Moreover, the sample absorbs energy from electromagnetic waves as they travel through the material until the energy of the electromagnetic waves is reduced to zero. As such, inner portions of the sample may never experience any electromagnetic waves when the sample quantity is too large [14,18].

### 3.2. Crystal structure analysis

#### 3.2.1. FESEM images of $Bi_{2x}Sb_{2(1-x)}Te_3$ ingots

$Bi_{2x}Sb_{2(1-x)}Te_3$ ingots were produced via solid-state microwave synthesis, as shown by the FESEM images in Fig. 2. Most of the grains had woody stems and were uniformly arranged, formed by the assembly of micro-sheet grains in a variety of sizes. The average size of the grains appeared to increase via Bi-substitution for Sb, indicating that Bi alloying is an effective approach for crystalline refinement. The samples (Figs. 2(d) to (f)) were nearly completely dense and no pores were observed. However, the grains and grain boundary morphologies varied with the Bi content ($x$). Thus, samples prepared using microwaves yielded products with different morphologies and microstructures [15,19].

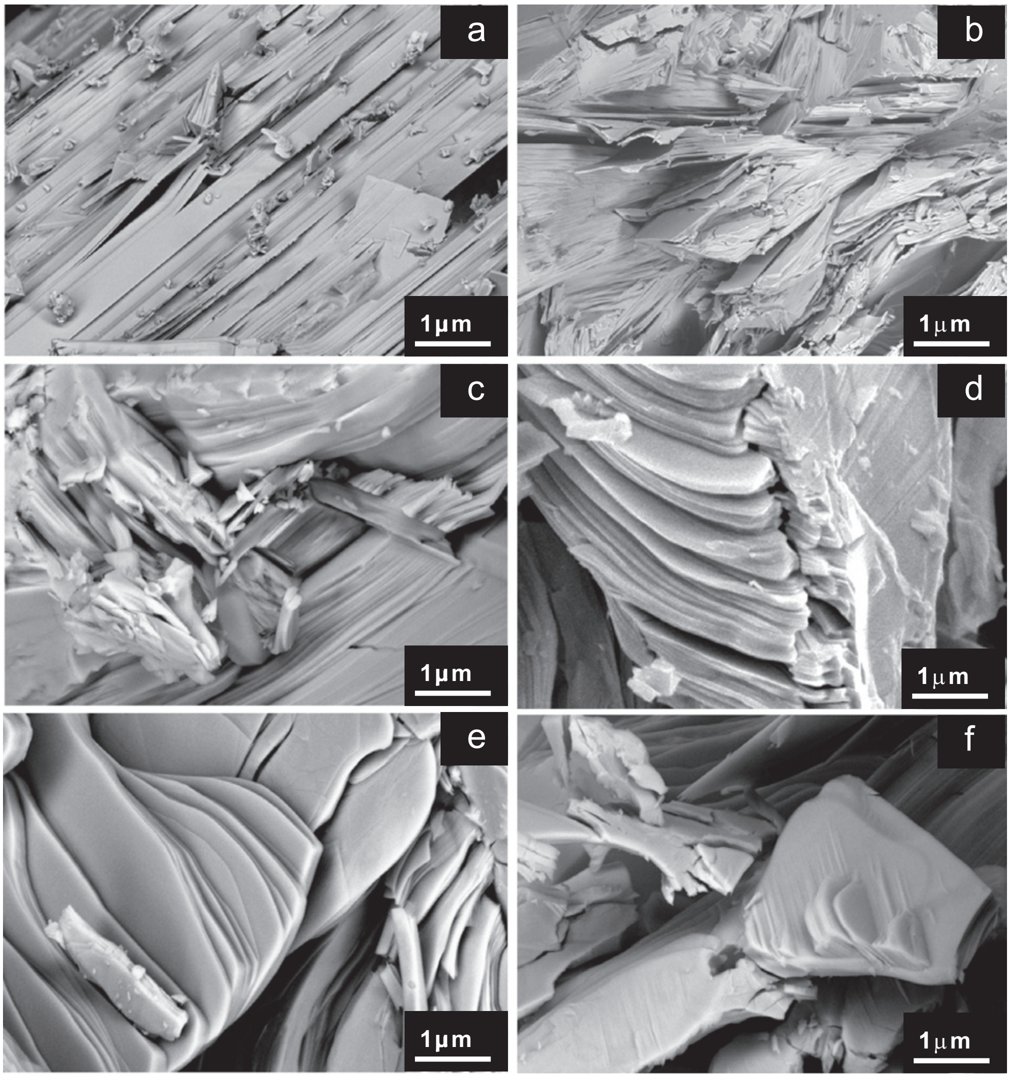

**Fig. 2.** Field emission scanning electron microscopy (FESEM) image of $Bi_{2x}Sb_{2(1-x)}Te_3$ ingots where (a) $x=0.0$, (b) $x=0.2$, (c) $x=0.4$, (d) $x=0.6$, (e) $x=0.8$, and (f) $x=1.0$.

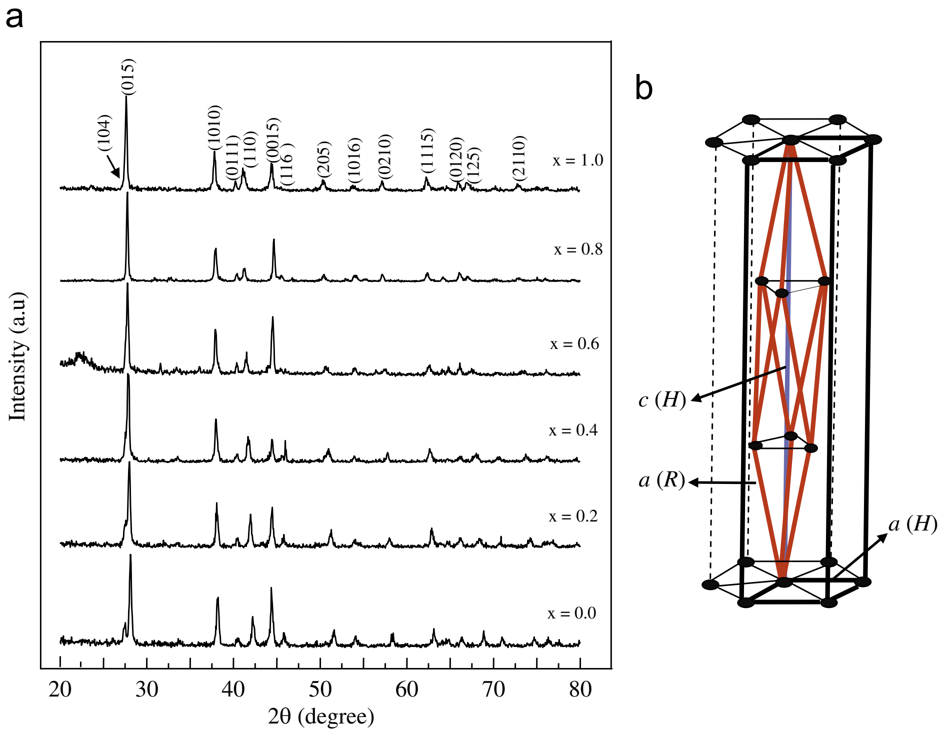

**Fig. 3.** (a) X-ray diffraction (XRD) patterns of $Bi_{2x}Sb_{2(1-x)}Te_3$ powders prepared via rapid solid-state microwave synthesis and (b) rhombohedral and hexagonal unit cells of the rhombohedral lattice.

### 3.2.2. XRD analysis of $Bi_{2x}Sb_{2(1-x)}Te_3$ powders

XRD spectra illustrated in Fig. 3(a) for the $Bi_{2x}Sb_{2(1-x)}Te_3$ powders indicate that the powders are polycrystalline and characterized by a rhombohedral structure (space group $R3m$), with a dominant peak representing the plane (0 1 5), agreeing well with the JCPDS values for $Sb_2Te_3$ and $Bi_2Te_3$ (Card Nos.15-0874 and 15-0863, respectively). No remarkable diffractions were found among other phases, indicating that pure $Sb_2Te_3$ and $Bi_2Te_3$ were obtained. The (0 0 15) orientation was generally strongly preferred, especially for samples with $x=0.0$, 0.6, and 0.8. The rhombohedral crystal structure can be represented as a stack of hexagonally arranged atomic layers, as shown in Fig. 3(b). The lattice constant of the rhombohedral unit cell $a(R)$ for the powders can be determined using the following relationship [20]:

$$a(R)=\frac{1}{3}\sqrt{3a(H)^2+c(H)^2} \tag{1}$$

where $a(H)$ and $c(H)$ are the lattice constants for the hexagonal phase structure. These lattice constants can be calculated using the following equation [20]:

$$\frac{1}{d^2}=\frac{4}{3}\left(\frac{h^2+hk+k^2}{a(H)^2}\right)+\frac{l^2}{c(H)^2} \tag{2}$$

As listed in Table 1, the diffraction peak (0 1 5) shifted to a lower $2\theta$ angle, from 28.12° to 27.64°, with increasing $x$, suggesting that the lattice parameter also increases with increasing $x$, likely due to substitution of Bi (~1.60 Å) for Sb (~1.45 Å). Thus, from the two XRD peaks, (0 1 5) and (1 0 10), $a(H)$ monotonically increases with increasing $x$, whereas $c(H)$ and $a(R)$ decrease for $x>0.4$. From these results, the solid-state microwave synthesis gives a reasonable indication that Bi atoms successfully occupy Sb sites in the as-prepared compounds.

### 3.3. Electrical transport properties

Fig. 4 shows $\sigma$ as a function of temperature for the $Bi_{2x}Sb_{2(1-x)}Te_3$ disks. The $\sigma$ of all samples decreased with increasing temperature, indicating that all samples display degenerate semiconductor characteristics and suggesting that the carriers are in an extrinsic state within the whole temperature range studied. At first, the relative densities of the samples were nearly identical (94%). Thus, the effect of sample density could be excluded. Two competing factors of carrier concentration and mobility determine electrical conductivity. Using the formula $\sigma=pe\mu$, $\sigma$ can be expressed in terms of carrier concentration. Generally, $\sigma$ decreases with increasing $x$. The values decreased from $8.6\times10^5$ S/m to $1.9\times10^5$ S/m at 303 K and from $3.8\times10^5$ S/m to $9.6\times10^4$ S/m at 523 K with $x$ increasing from 0.0 to 1.0, respectively. Compared with other samples, the sample with $x=0.2$ had a higher $\sigma$ ($9.6\times10^5$ S/m at 303 K and $4.8\times10^5$ S/m at 523 K). Therefore, differences in $\sigma$ could be ascribed to the different carrier concentrations caused by the compositions. This indicates that the microwave irradiation technique, combined with Bi as composition source ($x=0.2$), is more advantageous when increasing $\sigma$ of $Sb_2Te_3$ compared with traditional techniques [21].

Fig. 5 shows the $S$ of the $Bi_{2x}Sb_{2(1-x)}Te_3$ disks as a function of the measured temperature. The highest $S$ was 150 μV/K at 403 K for the sample with $x=1.0$. This result confirms the suggestion that the substitution of Bi for Sb in $Sb_2Te_3$ can result in possible decreases in both carrier

**Table 1**
Diffraction peak (0 1 5) and lattice parameters $a(H)$, $c(H)$, and $a(R)$ obtained through XRD analyses.

| $x$ | 0.0 | 0.2 | 0.4 | 0.6 | 0.8 | 1.0 |
|---|---|---|---|---|---|---|
| $2\theta^\circ$ | 28.12 | 27.985 | 27.889 | 27.809 | 27.79 | 27.64 |
| $a(H)$(Å) | 4.289 | 4.318 | 4.336 | 4.355 | 4.364 | 4.396 |
| $c(H)$(Å) | 30.50 | 30.51 | 30.54 | 30.51 | 30.41 | 30.43 |
| $a(R)$(Å) | 10.464 | 10.471 | 10.483 | 10.476 | 10.445 | 10.456 |

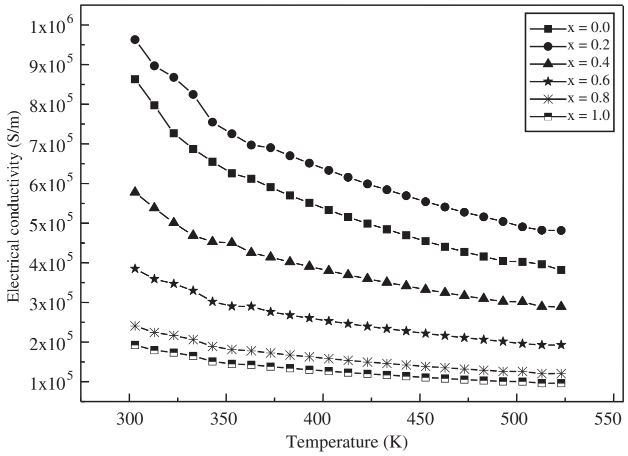

**Fig. 4.** Electrical conductivities as a function of temperature of $Bi_{2x}Sb_{2(1-x)}Te_3$ disks with different compositions.

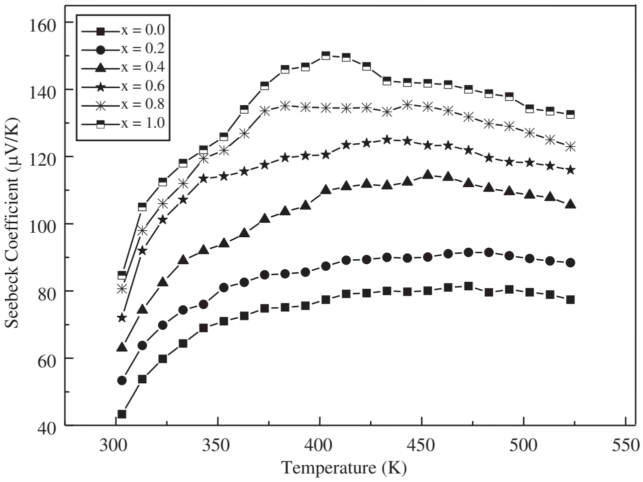

**Fig. 5.** Seebeck coefficients as a function of temperature of $Bi_{2x}Sb_{2(1-x)}Te_3$ disks with different compositions.

**Table 2**
Electrical conductivity $\sigma$, Hall coefficient $R_H$, carrier concentration $p$, and carrier mobility $\mu_H$ at room temperature of the samples with $x$=0.0, 0.2, 0.4, 0.6, 0.8, and 1.0.

| x | $\sigma \times 10^5$ (S/m) | $R_H$ ($cm^3$/C) | $p \times 10^{20}$ (1/$cm^3$) | $\mu_H$ ($cm^2$/V s) |
|---|---|---|---|---|
| 0.0 | 8.6 | 0.01488 | 4.2 | 126.480 |
| 0.2 | 9.6 | 0.01157 | 5.4 | 111.072 |
| 0.4 | 5.7 | 0.01894 | 3.3 | 107.958 |
| 0.6 | 3.8 | 0.02604 | 2.4 | 98.952 |
| 0.8 | 2.4 | 0.03289 | 1.9 | 78.936 |
| 1.0 | 1.9 | 0.04807 | 1.3 | 91.333 |

concentration and mobility. Samples with high $x$ exhibited relatively higher $S$. These results are in agreement with previously reported works [21,22]. $S$ values of all the samples were positive, indicating that the majority of the charge carriers are holes (p-type) within the measured temperature range. For degenerate semiconductors, $S$ can be described using the following equation:

$$S = \frac{8\pi^2 k_B^2}{3eh^2} m^* T \left(\frac{\pi}{3p}\right)^{2/3} \tag{3}$$

where $k_B$ is Boltzmann's constant, $h$ is Plank's constant, and $m^*$ is the effective mass. The relationship above shows that $S$ is highly dependent on the carrier concentration and increases with decreasing carrier concentration. Variations in $S$ are understood by assuming the scattering distance of the charge carrier independent of energy and degenerate approximations [23].

$R_H$ was measured via the van der Pauw method with a magnetic field strength of 1 T. The carrier concentration ($p$) and carrier mobility ($\mu_H$) may be calculated using the following equations: $p=1/e\ R_H$ and $\mu_H=\sigma/pe$. Table 2 shows the dependence of $R_H$ and $p$ of $Sb_2Te_3$ as a function of the $x$. The carrier concentration of $Sb_2Te_3$ decreased with increasing $x$, agreeing with previously reported results [21]. The carrier concentration for $Sb_2Te_3$ was $4.2 \times 10^{20}/cm^3$, slightly decreasing to $1.3 \times 10^{20}/cm^3$ for $Bi_2Te_3$. The sample with $x$=0.2 had a higher hole concentration ($5.4 \times 10^{20}/cm^3$), bringing about an increase in electrical conductivity. Aside from the composition dependence of the carrier concentration, the properties of chemical bonds significantly influenced carrier mobility. Generally, covalent bonds are more favorable for the transport of carriers compared with ionic bonds [24]. Based on the Pauling empirical formula and electronegativities of both bonding atoms, the proportion of the ionic component of the $A$–$B$ bond can be estimated using the following equation: $1-\exp[-(\chi_A-\chi_B)^2/4]$, where $\chi_A$ and $\chi_B$ are the electronegativities of the $A$ and $B$ atoms, respectively [25]. Based on the values of the electronegativities of the atoms Bi (2.02), Sb (2.05), and Te (2.10), the Bi–Te bond (0.16%) displays more ionic components than the Sb–Te bond (0.07%). Therefore, binary $Sb_2Te_3$, which possesses more covalent components, shows much higher carrier mobility (126.480 $cm^2$/V s) than binary $Bi_2Te_3$ (91.333 $cm^2$/V s). Moreover, with the incorporation of Bi into the binary $Sb_2Te_3$ compound, the carrier mobility first decreases because of the intensification of alloy scattering and gradual transformation of bond properties. Both the carrier concentration and mobility of the samples decreased at $x < 1.0$. During microwave irradiation, Te vaporization occurred, and antistructure defects were generated by the occupation of Sb and Bi atoms in vacant Te sites. With increasing $x$ ($x$=1.0), the concentration of the lattice defects decreased and the grain size increased (Fig. 2(f)), resulting in a decrease in scattering of lattice defects to the carrier (subdued alloy scattering). Hence, the carrier mobility increased [21,26].

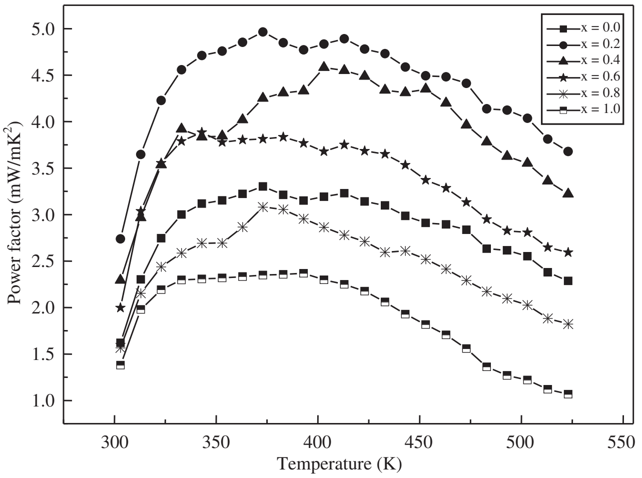

**Fig. 6.** Power factors as a function of temperature of $Bi_{2x}Sb_{2(1-x)}Te_3$ disks with different compositions.

A decrease in the difference in electronegativity between the component atoms is favorable for the formation of antistructure defects. Hence, the carrier (hole) concentration of $Bi_{2x}Sb_{2(1-x)}Te_3$ decreased with increasing $Bi_2Te_3$ content because fewer antistructure defects were formed given the larger difference in electronegativity between Bi and Te than that between Sb and Te [21,27].

Based on the data obtained above, the temperature dependence of $\sigma S^2$ for $Bi_{2x}Sb_{2(1-x)}Te_3$ compounds is shown in Fig. 6. The temperature behaviors of $\sigma S^2$ for the six samples are similar: increasing with increasing temperature, achieving a maximum, and then decreasing with further increases in temperature. $\sigma S^2$ values obtained for $x=0.2$, 0.4, and 0.6 were larger than those for $x=0.0$, 0.8, and 1.0 within the entire temperature range investigated. $\sigma S^2$ for the $x=0.2$ sample was 4.96 mW/mK$^2$ at 373 K, whereas the maximum $\sigma S^2$ for samples with $x=0.0$ and 1.0 were 3.30 mW/mK$^2$ at 373 K and 2.37 mW/mK$^2$ at 393 K, respectively. Good TE properties for $x=0.2$ originated from the relatively high $\sigma$ of the sample.

## 4. Conclusions

P-type $Bi_{2x}Sb_{2(1-x)}Te_3$ ingots with six chemical compositions ($x=0.0$, 0.2, 0.4, 0.6, 0.8, and 1.0) were prepared via solid-state microwave synthesis. As-synthesized ingots exhibited a woody stem-like structure. By increasing $x$ in the Bi–Sb–Te system, the hole concentration decreased and caused an increase in $S$ and a decrease in $\sigma$. The maximum $\sigma S^2$ measured was significantly improved from 3.30 mW/mK$^2$ for the $Sb_2Te_3$ sample to 4.96 mW/mK$^2$ for the $Bi_{0.4}Sb_{1.6}Te_3$ sample. The sample at $x=0.2$ exhibited improved TE properties. The preparation route proposed in this work to yield $Sb_2Te_3$-based materials is low cost and promising.

## Acknowledgment

The authors would like to thank Dr. Ng Eng Poh and Mr. Jamal Mohamed from the School of Chemical Sciences at the Universiti Sains Malaysia for helping us overcome some of the obstacles we met during the completion of this research. This work was supported by the Postgraduate Research Grant Scheme (PRGS) 1001/PFIZIK/844091 of the Universiti Sains Malaysia.

## References

[1] H. Muguerra, B. Rivas-Murias, M. Traianidis, C. Henrist, B. Vertruyen, R. Cloots, Journal of Solid State Chemistry 183 (2010) 1252–1257.
[2] J.J. Shen, S.N. Zhang, S.H. Yang, Z.Z. Yin, T.J. Zhu, X.B. Zhao, Journal of Alloys and Compounds 509 (2011) 161–164.
[3] L.M. Goncalves, P. Alpuim, M. Gao, D.M. Rowe, C. Couto, J.H. Correia, Vacuum 82 (2008) 1499–1502.
[4] L.I. Soliman, M.M. Nassary, H.T. Shaban, A.S. Salwa, Vacuum 85 (2010) 358–364.
[5] J.L. Cui, H.F. Xue, W.J. Xiu, L.D. Mao, P.Z. Ying, L. Jiang, Journal of Alloys and Compounds 460 (2008) 426–431.
[6] P. Rauwel, O.M. Lovvik, E. Rauwel, J. Tafto, Acta Materialia 59 (2011) 5266–5275.
[7] D.B. Hyyn, T.S. Oh, J.S. Hwang, J.D. Shim, N.V. Kolomoent, Scripta Materialia 40 (1999) 49–56.
[8] J. Yang, T. Aizawa, A. Yamamoto, T. Ohta, Journal of Alloys and Compounds 309 (2000) 225–228.
[9] X.A. Fan, J.Y. Yang, W. Zhu, H.S. Yun, R.G. Chen, S.Q. Bao, et al., Journal of Alloys and Compounds 420 (2006) 256–259.
[10] J. Seo, K. Park, D. Lee, C. Lee, Scripta Materialia 38 (1998) 477–484.
[11] C.D. Moon, S. Shin, D.H. Kim, T. Kim, Journal of Alloys and Compounds 504 (2010) S504–S507.
[12] Z. Zhang, D. Gekhtman, M.S. Dresselhaus, J.Y. Ying, Chemistry of Materials 11 (1999) 1659.
[13] A. Kadhim, A. Hmood, H. Abu Hassan, Materials Letters 65 (2011) 3105–3108.
[14] C. Mastrovito, J.W. Lekse, J.A. Aitken, Journal of Solid State Chemistry 180 (2007) 3262–3270.
[15] A.G. Whittaker, Chemistry of Materials 17 (2005) 3426–3432.
[16] R. Roy, D. Agrawal, J. Cheng, S. Gedevanishvili, Nature 401 (1999) 304.
[17] M. Jeselnik, R.S. Varma, S. Polanc, M. Kocevar, Green Chemistry 4 (2002) 35–38.
[18] J.W. Lekse, A.M. Pischera, J.A. Aitken, Materials Research Bulletin 42 (2007) 395–403.
[19] U.R. Pillai, E. Sahle-Demessie, R.S. Varma, Applied Catalysis A: General 252 (2003) 1.
[20] B.D. Cullity, Element of X-ray Diffraction, 3rd edn., Wesley Publishing Company, USA, 1967.
[21] J. Jiang, L. Chen, S. Bai, Q. Yao, Q. Wang, Journal of Crystal Growth 277 (2005) 258–263.
[22] D. Li, R.R. Sun, X.Y. Qin, Intermetallics 19 (2011) 2002–2005.
[23] S. Wang, W. Xie, H. Li, X. Tang, Intermetallics 19 (2011) 1024–1031.
[24] G.J. Snyder, E.S. Toberer, Nature Materials 7 (2008) 105–114.
[25] M.L. Bhatia, Intermetallics 7 (1999) 641–651.
[26] X.A. Fan, J.Y. Yang, R.G. Chen, W. Zhu, S.Q. Bao, Materials Science and Engineering A 438–440 (2006) 190–193.
[27] J. Horak, K. Cermak, L. Koudelka, Journal of Physics and Chemistry of Solids 47 (1986) 805.